C. T.-C. Nguyen and R. T. Howe, "Electromechanical characterization of microresonators for circuit applications," *Tech. Dig.*, MICRO Program, 1991.

Electromechanical Characterization of Microresonators for Circuit Applications

Tu-Cuong H. Nguyen and Roger T. Howe

University of California at Berkeley
Department of Electrical Engineering and Computer Sciences
and the Electronics Research Laboratory
Berkeley, California 94720

Final Report 1990-91, MICRO Project#89-162
Industrial Sponsor: General Motors

Abstract

The design of circuits incorporating microresonators which utilize electrostatic drive and sense is accompanied by a need for a convenient method to experimentally extract the circuit elements modelling the microresonators. Previously, techniques which *electrically* detect microresonator motional current using only *off-chip* electronics have been seriously hampered by parasitic feedthrough currents arising from probe-to-probe capacitance, which mask the tiny motional current. This paper details a novel technique which allows *off-chip electrical* determination of a microresonator transconductance spectrum by separating motional current from feedthrough in the frequency domain; effectively, it eliminates all dc capacitance and senses only ac (motional) capacitance. Application of this technique to microresonator circuit model extraction and system performance verification will be demonstrated.

I. Introduction

Mechanical resonators have proven to be highly sensitive probes for physical or chemical parameters which alter their potential or kinetic energy. This sensitivity, usually occuring as a resonance frequency shift, has been harnessed by recent microfabricated sensors, which utilize resonant micromechanical structures as transducing elements [1, 2, 3]. Microsensors for detecting pressure [4, 5], acceleration [6], and vapor concentration [7] have been demonstrated. In addition to the aforementioned sensor applications, the high quality factor Q of microresonators in vacuum suggests a strong potential for use as frequency references in monolithic systems and as electromechanical filters.

The design of circuits incorporating microresonators which utilize electrostatic drive and sense is accompanied by a need for a convenient method to experimentally extract the circuit elements modelling the microresonators. The equivalent circuit for an electrostatic-comb driven microresonator biased and excited as in Fig. 1 is presented in Fig. 2, which includes expressions for calculating the elements. The circuit elements are primarily determined by the resonance frequency ω_r, the quality factor Q, and the change in finger overlap capacitance per unit displacement $\frac{\partial C}{\partial x}$. The last two of these parameters are particularly difficult to determine theoretically, since they depend heavily upon second order effects. For example, Q depends upon the energy dissipation mechanisms in the system, of which Couette flow is the dominant, but not the only, mechanism of importance [8]. $\frac{\partial C}{\partial x}$ is even more difficult to predict, since it is strongly influenced by both fringing electric fields and by bias-induced levitation of the movable shuttle [9]. These parameters, however, can be readily determined from an electrically measured microresonator transconductance spectrum.

Historically, implementation of a convenient, off-chip, open-loop, electrical characterization technique for capacitively excited and sensed microresonators has been difficult. To start, the motional current to be detected is miniscule, on the order of picoamperes for low Q (air-damped) situations. Furthermore, feedthrough currents arising from parasitic capacitance between probes contacting the drive and sense ports mask the motional current of the dc-biased oscillating structure. Thus, partially successful attempts to detect resonance electrically have been limited to the use of on-chip circuitry or the use of special, tedious precautions, including the requirement of operation in vacuum, to attenuate parasitic feedthrough [10].

The above restrictions to *electrical* transfer function measurement

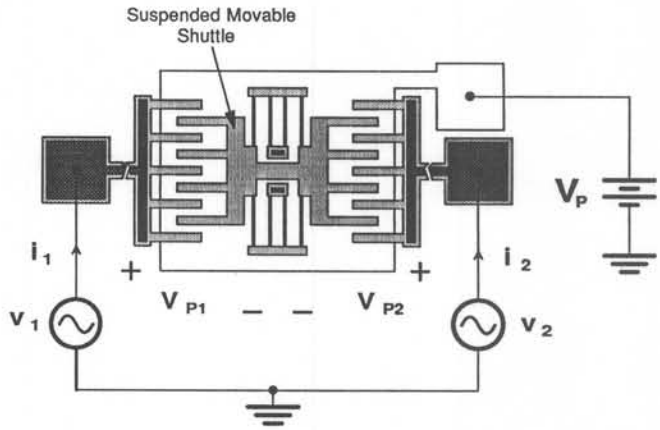

Fig 1. General bias and excitation for a two-port electrostatic-comb driven lateral microresonator. The dark shading indicates the points at which contact to the substrate (or ground plane) is made, while the more lightly shaded areas are suspended 2 μm above. The movable shuttle is anchored to the ground plane, and thus, is in electrical contact with it.

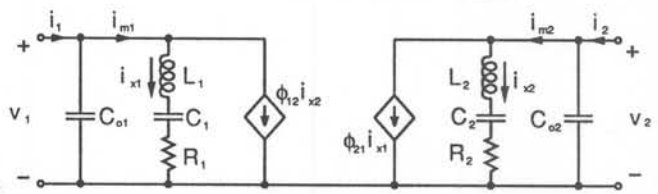

$$C_{o1} = C_{overlap1} \text{ at dc} \qquad C_{o2} = C_{overlap2} \text{ at dc}$$

$$L_1 = \frac{k_{sys}}{\omega_r^2 V_{P1}^2 \left(\frac{\partial C}{\partial x}\right)_1^2} \qquad L_2 = \frac{k_{sys}}{\omega_r^2 V_{P2}^2 \left(\frac{\partial C}{\partial x}\right)_2^2}$$

$$C_1 = \frac{V_{P1}^2}{k_{sys}} \left(\frac{\partial C}{\partial x}\right)_1^2 \qquad C_2 = \frac{V_{P2}^2}{k_{sys}} \left(\frac{\partial C}{\partial x}\right)_2^2$$

$$R_1 = \frac{k_{sys}}{\omega_r Q V_{P1}^2 \left(\frac{\partial C}{\partial x}\right)_1^2} \qquad R_2 = \frac{k_{sys}}{\omega_r Q V_{P2}^2 \left(\frac{\partial C}{\partial x}\right)_2^2}$$

$$\phi_{12} = \frac{V_{P1}\left(\frac{\partial C}{\partial x}\right)_1}{V_{P2}\left(\frac{\partial C}{\partial x}\right)_2} \qquad \phi_{21} = \phi_{12}^{-1} = \frac{V_{P2}\left(\frac{\partial C}{\partial x}\right)_2}{V_{P1}\left(\frac{\partial C}{\partial x}\right)_1}$$

Fig 2. Equivalent circuit for the microresonator of Fig. 1 with expressions for the elements. Typical element values for low-Q (Q = 27) operation of a microresonator with f_r = 17.2 kHz are C_o = 4.25 fF, L = 0.178 MH, C = 0.482 fF, and R = 712 M Ω.

have led to *optical* techniques [11], in which laser light, reflected from an oscillating microstructure, is detected. However, optical techniques suffer from several drawbacks. First, alignment of laser light, even via optical fibers, is a tedious affair, making transfer function determination somewhat inconvenient from structure to structure. Second, special, more expensive equipment is necessary for high-Q vacuum applications, since it is difficult to feed a fiber into a vacuum environment. Finally, and most importantly, actual *electrical* information is not provided; important information concerning the electrical performance of capacitively driven and sensed microstructures (as used in sensors, oscillators, etc.) is lacking, and thus, direct performance verification of electronic systems utilizing microresonators is not possible.

This paper details a novel technique which allows *off-chip electrical* determination of a microresonator transconductance spectrum by separating motional current from feedthrough in the frequency domain and providing amplification for the former. These are achieved by applying a high frequency ac signal (on top of the dc bias) to the microstructure. This signal serves as a carrier which is modulated by the time-varying sense capacitance of the resonating structure, therefore, separating motional current from dc feedthrough in the frequency domain. Even the intrinsic dc capacitance of the microstructure is effectively eliminated.

This electromechanical amplitude modulation (EAM) technique is useful for one-port, as well as multi-port, microstructures with virtually any range of Q. It has been successfully demonstrated as a convenient, repeatable, wafer-level measurement technique and shows potential for application in integrated detection circuitry.

In addition to providing a detailed description of the EAM characterization technique, this paper will also demonstrate its application to microresonator circuit model extraction and system performance verification (for the case of a microelectromechanical filter). First, however, parasitic feedthrough interference and its role in dictating feasible detection techniques is discussed.

II. Parasitic Feedthrough Interference

Figure 3 shows a typical probe placement scheme for direct off-chip detection of microresonator motional current i_s. Typical values for the probe-to-probe parasitic capacitor are given for the case of unshielded tungsten probes and (in parentheses) for the case of coaxial probes. Note that these parasites are generally larger than the variation in capacitance of an oscillating microresonator, which is usually on the order of one femtofarad or less.

Parasitic feedthrough causes distortion in the series resonant transconductance spectrum of a microresonator. This is readily seen in Fig. 4, where simulated transconductance vs. frequency plots are presented for the microresonator of Fig. 3 (assuming operation at atmospheric pressure) under two conditions: (a) all dc capacitors, including the intrinsic device dc capacitance, neglected; and (b) all dc capacitors, including parasites, included. Case (a) depicts pure series resonance and is ideal for characterization purposes, since it readily provides resonance frequency ω_r, quality factor Q, and $\frac{\partial C}{\partial x}$. Case (b), which models the detection scheme of Fig. 3, shows heavy distortion of the desired spectrum. Such distortion makes Q difficult to extract and alters the performance of microresonator systems—in particular, of microelectromechanical filters.

The degree to which parasitic feedthrough masks motional current, causing distortion, is a function of the voltage required to drive the microresonator (as well as the amount of parasitic capacitance), and thus, is a function of the Q of the system. For very high vacuum operation, where ac drive voltages as small as 1 mV in amplitude might suffice, the motional current of a microresonator can be be detected directly. However, as the Q goes down, and the required ac voltage becomes larger, motional current masking quickly makes *direct* off-chip detection of resonance difficult.

An idea of the voltage magnitude threshold allowing detection by direct methods (Fig. 3) can be conveniently provided by Fourier spectra obtained via the recent gated-sinusoid excitation and detection (GSED) scheme [12], which allows detection of resonance in microstructures under medium- to high-Q conditions, but does not allow measurement of a transconductance spectrum. Briefly, the technique involves exciting the microstructure with a gated (pulsed) sinusoid, driving the structure during the sinusoid portion of excitation, and detecting during the zero input portion. Measurements on low frequency ($f_r = 20$ kHz) microresonators using GSED conclude that ac voltage amplitudes on the order of tens of millivolts define the threshold whereby motional current can be measured with acceptable interference from probe-to-probe parasitics, and spectra similar to that in Fig. 4(a) can be obtained. For one-port microresonators, however, where there is an intrinsic dc capacitance in parallel with the motional capacitance, a spectrum distorted from pure series resonance (although not as heavily distorted as Fig. 4(b) if done in high vacuum) will always result when a direct off-chip detection technique is used. For this case, and for the case of medium- to low-Q measurements or for systems requiring voltage swings larger than tens of millivolts (e.g. systems where the microresonator has a large spring constant), a technique which nulls dc capacitance is desired. EAM provides such a technique.

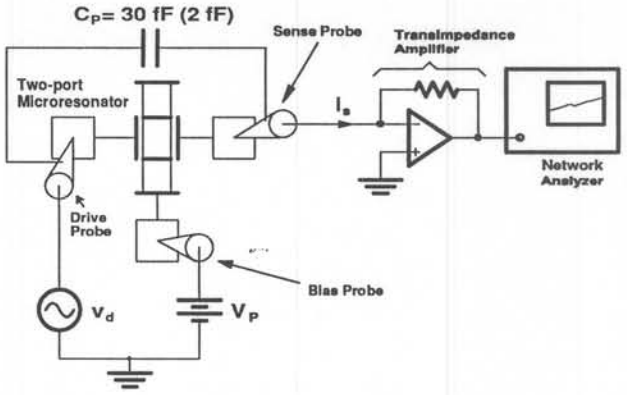

Fig 3. Experimental set-up for direct off-chip detection of microresonator motional current. This detection strategy is ineffective when drive voltages larger than a few millivolts are required because of interference from probe-to-probe parasitic feedthrough. (Here, the circuit symbol for a two-port microresonator, which readily corresponds to the drawing in Fig. 1, is used.)

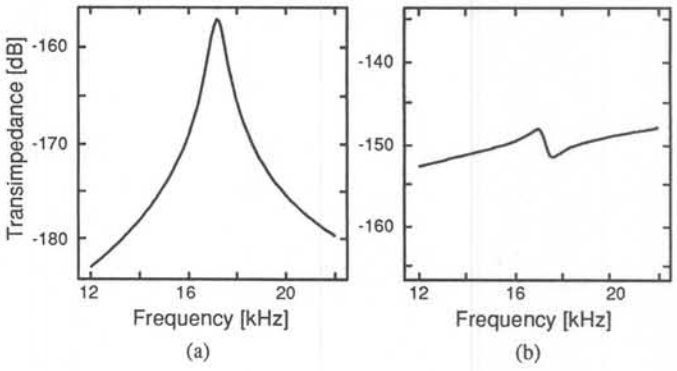

Fig 4. (a) Simulated transconductance spectrum for a microresonator biased as in Fig. 3 but under the assumption of no parasitic capacitance. (b) Simulated transconductance spectrum for the microresonator of Fig. 3 including probe-to-probe parasitic capacitance.

III. Electromechanical Amplitude Modulation (EAM)

The GSED technique enables motional current detection by separating it from feedthrough current in the *time domain*. Electromechanical amplitude modulation (EAM), on the other hand, separates motional and feedthrough current in the *frequency domain*. A circuit schematic for EAM is presented in Fig. 5 for the case of a two-port microresonator. Parasitic capacitors, C_{PD} and C_{PC}, due to probe tips and surface dielectrics, are also included.

The key to EAM lies in the biasing of the microstructure, which includes an ac carrier signal, as well as the dc-bias required for drive force amplification. Qualitatively, the carrier signal and its time-derivative are multiplied by capacitive elements of microstructure motion, resulting in motional current, frequency-shifted to sidebands around the carrier frequency and separated from dc parasites still at the driving frequency.

The principle mechanisms involved in electromechanical amplitude modulation will now be derived.

IV. The EAM Sidebands

The Fourier spectrum for the sense current i_s in Fig. 5 will now be derived for the case of a two-port electrostatic-comb driven lateral microresonator. This current is given by (refer to Fig. 5)

$$i_s = C_{PD}\frac{dV_f(t)}{dt} + C_{PC}\frac{dV_s(t)}{dt} + C(t)\frac{dV_s(t)}{dt} + V_s(t)\frac{dC(t)}{dt} \quad (1)$$

where

$$C(t) = \begin{cases} \approx C_o & \text{off resonance} \\ C_o + C_m(t) & \text{at resonance} \end{cases} \quad (2)$$

$$C_m(t) = |C_m| \sin \omega_r t \quad (3)$$

where $C(t)$ represents the microresonator finger-overlap capacitance at the *sense port*, C_o is the dc value of this capacitance, $C_m(t)$ is the motional (ac value of) capacitance at the sense port, and C_{PD} and C_{PC} are parasitic capacitors (comprised mainly of probe-to-probe capacitance).

Solving Eq. (1) at resonance, using the appropriate condition of Eq. (2) and setting $\omega_d = \omega_r$ (r for resonance), the current entering the summing node of the transimpedance amplifier i_s is found to be

$$\begin{aligned} i_r &= i_P - \omega_r V_P |C_m| \cos\omega_r t \\ &\quad + \frac{1}{2}(\omega_c - \omega_r)|C_m||v_c|\cos(\omega_c - \omega_r)t \\ &\quad - \frac{1}{2}(\omega_c + \omega_r)|C_m||v_c|\cos(\omega_c + \omega_r)t. \end{aligned} \quad (4)$$

where i_P represents components of current feeding through dc capacitors (predominantly parasitics). The current peaks (in the Fourier spectrum) due to motion of the microstructure are those containing the time-varying capacitance amplitude term, $|C_m|$. The motional currents of interest, however, are only those at frequencies $(\omega_c - \omega_r)$ and $(\omega_c + \omega_r)$, since the motional current at ω_r is inaccessible due to masking by feedthrough currents. The amplitudes of these sidebands are readily seen from Eq. (4) to be given by

$$|I_{LHS}| = \frac{1}{2}(\omega_c - \omega_r)|C_m||v_c| \quad (5)$$

$$|I_{RHS}| = \frac{1}{2}(\omega_c + \omega_r)|C_m||v_c|. \quad (6)$$

These equations show that the left-hand and right-hand sidebands of motional current are not equal in amplitude. The Fourier spectrum corresponding to Eq. (4) for i_s at resonance is presented in Fig. 6(a).

Equations (5) and (6) may be converted to useful transconductance equations, relating phasor sense current I_s to phasor drive voltage V_d, given an expression for $|C_m|$. Such an expression has been derived elsewhere [12] through consideration of an explicit form for $\frac{\partial C}{\partial t}$, and the result is simply presented here:

$$|C_m| = V_P \frac{Q}{k_{sys}}\left(\frac{\partial C}{\partial x}\right)_d\left(\frac{\partial C}{\partial x}\right)_s V_d. \quad (7)$$

where k_{sys} is the system spring constant, and $\left(\frac{\partial C}{\partial x}\right)_d$ and $\left(\frac{\partial C}{\partial x}\right)_s$ correspond to the drive and sense ports, respectively. Substitution of (7) in Eqs. (5) and (6) yields the transconductance functions at resonance relating phasor sense current I_s and phasor drive voltage V_d for each sideband of motional current:

$$\left|\frac{I_{LHS}}{V_d}\right| = \frac{1}{2}(\omega_c - \omega_r)|v_c|V_P\frac{Q}{k_{sys}}\left(\frac{\partial C}{\partial x}\right)_d\left(\frac{\partial C}{\partial x}\right)_s \quad (8)$$

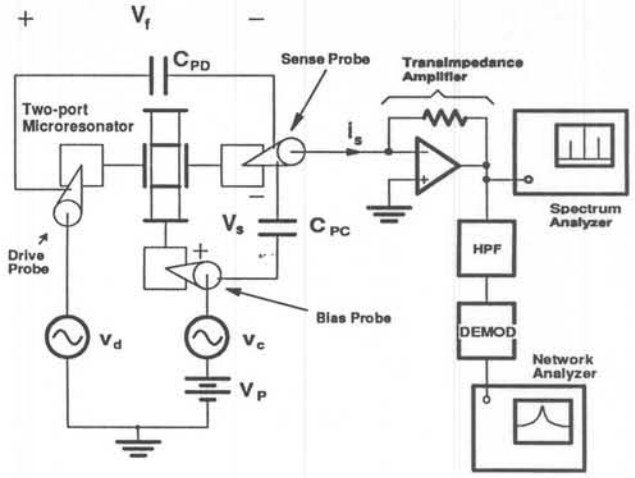

Fig 5. Schematic of the EAM system for determination of a microresonator transconductance spectrum.

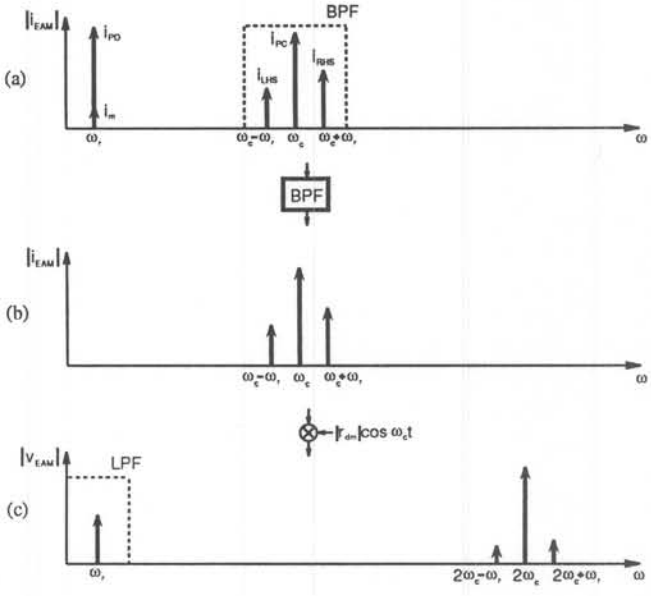

Fig 6. Schematic flow diagram of the post-processing necessary to prepare the EAM current i_{EAM} for input to a network analyzer. (a) A bandpass filter is used to filter out the components at the drive frequency. This filtering also improves the signal-to-noise ratio of the system. (b) The sidebands are demodulated back down to the drive frequency with a sinusoid at the carrier frequency ω_c and with adjustable phase. (c) Final EAM output suitable for input to a network analyzer. For viewing with an oscilloscope, the lowpass filter will be necessary.

$$\left|\frac{I_{RHS}}{V_d}\right| = \frac{1}{2}(\omega_c + \omega_r)|v_c|V_P\frac{Q}{k_{sys}}\left(\frac{\partial C}{\partial x}\right)_d\left(\frac{\partial C}{\partial x}\right)_s \quad (9)$$

The magnitude of the transconductance at resonance of a dc-biased (*no ac*) electrostatic-comb driven lateral microresonator has been reported previously to be [8]:

$$\left|\frac{I_s}{V_d}\right| = \omega_r V_P^2\frac{Q}{k_{sys}}\left(\frac{\partial C}{\partial x}\right)_d\left(\frac{\partial C}{\partial x}\right)_s \quad (10)$$

Comparison of (10) with Eqs. (8) and (9) shows that motional current produced via EAM contains a $\frac{1}{2}(\omega_c \pm \omega_r)$ factor replacing the ω_r term of oscillating dc-biased structures. Thus, motional current produced via EAM is amplified over that produced by an oscillating dc-biased (*only*) structure by a factor of approximately $\frac{\omega_c|v_c|}{2\omega_r V_P}$ (for $\omega_c \gg \omega_r$, which is usually the case). Since the carrier frequency may be selected arbitrar-

ily large (the limitation coming from the bandwidth of post-processing electronics), this amplification can be very large.

V. Demodulation of EAM Motional Current

In order to view the transconductance spectrum of the microresonator under a network analyzer, the EAM motional current i_{EAM} must be post-processed by *off-chip* electronics. Figure 6 summarizes the required signal processing.

The first step (Fig. 6(a)–(b)) involves a transimpedance amplification and bandpass filtering to eliminate the parasitic feedthrough component at the drive frequency ω_r (assuming resonance). Such filtering also enhances the signal-to-noise ratio of the sensing electronics.

Next (Fig. 6(b)–(c)), the EAM components of current i_{RHS} and i_{LHS} must be demodulated back down to the resonance frequency ω_r, yielding finally, the Fourier spectrum shown in Fig. 6(c). The spectrum in (c) is suitable for input to a network analyzer even without the lowpass filtering shown. The lowpass filter, however, is necessary for viewing via an oscilloscope.

Let us now focus on the demodulation of the EAM motional current back to the original microstructure oscillation frequency. As with any amplitude-modulated signal, this can be achieved by multiplication with a sinusoid of the carrier frequency ω_c. Unlike other demodulated signals, however, the magnitude (and phase) of the EAM output voltage $|V_{EAM}|$ depends upon the phase of the demodulating signal r_{dm}. Careful consideration should be given to selection of the proper phase for maximum EAM output.

To see this, let us now obtain an expression for the amplitude of v_{EAM} as a function of the phase θ of r_{dm}, generalized as

$$r_{dm} = |r_{dm}| \cos(\omega_c t + \theta). \tag{11}$$

Multiplication of Eq. (11) with (4), taking only motional current terms at ω_r, and converting to phasor form, yields:

$$V_{EAM} = |V_{EAM}| e^{\angle V_{EAM}} \tag{12}$$

where

$$|V_{EAM}| = \frac{1}{2}|C_m||v_c||r_{dm}|\sqrt{\omega_r^2 \cos^2\theta + \omega_c^2 \sin^2\theta} \tag{13}$$

$$\angle V_{EAM} = \tan^{-1}\left(-\frac{\omega_c \sin\theta}{\omega_r \cos\theta}\right). \tag{14}$$

The θ corresponding to the maximum V_{EAM} amplitude can be found by setting the derivative of $|V_{EAM}|$ to zero and solving for θ, yielding:

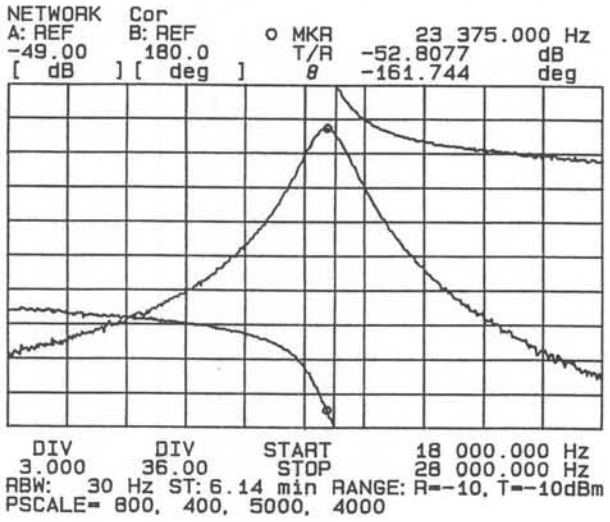

Fig 7. Transconductance spectrum for an electrostatic-comb driven lateral microresonator as determined by the EAM technique under atmospheric pressure.

$$\frac{\partial|V_{EAM}|}{\partial\theta} = \frac{2(\omega_c^2 - \omega_r^2)\sin\theta\cos\theta}{\sqrt{\omega_r^2\cos^2\theta + \omega_c^2\sin^2\theta}} = (\omega_c^2 - \omega_r^2)\sin\theta\cos\theta = 0. \tag{15}$$

From Eq. (15), $|V_{EAM}|$ is maximized when $\theta = 0°$ or $90°$, depending upon which of ω_c and ω_r is larger.

For the usual case where $\omega_c \gg \omega_r$, $|V_{EAM}|$ is maximized for $\theta = 90°$. Evaluating Eq. (13) at $\theta = 90°$, the maximum v_{EAM} is found to be

$$v_{EAM} = \frac{1}{2}\omega_c|C_m||v_c||r_{dm}| \sin\omega_r t. \tag{16}$$

Note that the maximum output signal is amplified over the output obtained directly from a dc-biased (only) microresonator by $\frac{\omega_c|v_c|}{2\omega_r V_P}$, assuming identical transimpedance amplification for both cases. In addition, unlike the output from a dc-biased (only) microresonator, the EAM demodulator output is 90° phase-shifted from the input signal v_d.

In summary, to maximize the output of the EAM demodulator, a demodulation signal 90° phase-shifted from the EAM carrier $r_{dm} = |r_{dm}| \sin\omega_c t$ is required. Such a demodulation signal yields an output with amplitude proportional to the carrier frequency and with phase 90° shifted from the drive signal.

VI. Microresonator Circuit Extraction

Figure 7 presents the transconductance spectrum for an electrostatic-comb driven microresonator operated in air as measured via the EAM technique. The spectrum depicts pure series resonance, indicating that all dc capacitance in parallel with the microresonator has been effectively nulled. It is ideal for microresonator circuit extraction, since it readily provides values for resonance frequency ω_r and quality factor Q. $\frac{\partial C}{\partial x}$ can also be easily obtained via the equation

$$\left(\frac{\partial C}{\partial x}\right)_s = \frac{2|\frac{V_{EAM}}{V_d}|N_s k_{sys}}{\omega_c V_P |v_c||r_{dm}|N_d Q} \tag{17}$$

where N_d and N_s are the number of fingers at the drive port and sense ports, respectively. Once these three parameters have been determined, the circuit elements modelling the microresonator in question can be readily calculated using the equations in Fig. 2. The differences between the extracted model and that obtained through simple theory (which ignores fringing fields and bias-induced shuttle levitation, and predicts Q assuming only Couette dissipation) can be very large [12]. The large discrepancy in the measured and derived elements, in particular that for resistance, results mainly from an underestimation by theory of the value of $\frac{\partial C}{\partial x}$ and a large overestimation of Q.

In addition to providing a means for experimental circuit extraction, the EAM transconductance spectrum can also provide valuable design information. For illustration, let us consider ground plane design for maximizing $\frac{\partial C}{\partial x}$, thus, minimizing the series resistance R. The peak current for a microresonator at resonance is strongly dependent upon the type of microresonator ground plane used. This dependence is caused by levitation of the microresonator shuttle due to a ground plane-induced imbalance of vertically directed electrostatic forces [9]. The amount of levitation determines the finger overlap capacitance, which in turn determines the value of $\frac{\partial C}{\partial x}$. The EAM technique along with Eq. (17) measures a 33% increase in $\frac{\partial C}{\partial x}$ when a striped ground plane instead of a full ground plane is utilized for a microresonator with 12 drive and sense fingers, thickness = 2 μm, finger gap = 2 μm, and f_r = 18.9 kHz, operated under low-Q conditions. This translates to a 44% decrease in series resistance R.

VII. Microresonator System Performance Verification

Possibly the most useful application of EAM is for off-chip verification of microresonator system performance. To illustrate, we take the parallel microresonator electromechanical filter, shown in Fig. 8. Such a filter operates through the addition of properly phased current outputs of microresonators with resonance frequencies differing by a specific amount [12], and thus, its performance may only be verified by an *electrically*-based sensing scheme.